Dark matter and collider phenomenology with two light supersymmetric Higgs bosons

Dan Hooper[1] and Tilman Plehn[2]

[1]*Department of Astrophysics, University of Oxford, Keble Road, Oxford OX1-3RH, United Kingdom*
[2]*Max Planck Institut fur Physik, Fohringer Ring 6, 80805 Munchen, Germany*

(Received 9 June 2005; revised manuscript received 11 August 2005; published 9 December 2005)

It has been suggested that two different excesses of events observed at CERN LEP could be interpreted as the CP-even Higgs bosons of the minimal supersymmetric standard model (MSSM) with masses of approximately 98 and 114 GeV. If this is the case, the entire MSSM-Higgs sector is required to be light. In this article, we explore such a scenario in detail. We constrain the Higgs and supersymmetric spectrum using B physics constraints as well as the magnetic moment of the muon. We then point out the implications for neutralino dark matter—next generation direct detection experiments will be sensitive to all MSSM models with such a Higgs sector. Finally, we find that all models outside a very narrow corridor of parameter space have a charged Higgs boson which will be observed at the CERN LHC. In those exceptional models which do not contain an observable charged Higgs, a light top squark will always be seen at the LHC, and likely at the Tevatron.

DOI: 10.1103/PhysRevD.72.115005 PACS numbers: 14.80.Cp, 12.60.Jv, 14.80.Ly, 95.35.+d

I. SETTING THE STAGE

All four experiments at LEP have searched for Higgs bosons up to a mass of approximately 115 GeV. Although no strong indication of a Higgs has been detected by LEP, excesses have been reported for Higgs-like events corresponding to masses of 98 and 115 GeV, respectively. While historically the combination of the four LEP experiments has weakened the four-jet excess at 115 GeV (dominated by ALEPH), it has strengthened the 98 GeV ''signal'' significance (with the strongest evidence from L3). The current background fluctuation probability is 2% or 2.3σ for the excess at 98 GeV and 9% or 1.7σ for its 115 GeV counterpart [1]. Very recently, it has been discussed by Drees how both of these excesses reported by LEP could be accommodated within the minimal supersymmetric standard model (MSSM) as signatures of the two CP-even Higgs bosons (without any modifications to the MSSM setup) [2,3].

One of the reasons that the LEP excess at 98 GeV has received so little attention might be that the rate observed at this mass is far below what we would expect from a standard model Higgs boson. In the MSSM, however, the h-Z-Z coupling is suppressed relative to the value in the standard model by a factor of $\sin(\beta - \alpha)$, where α is the mixing angle between the two CP-even Higgs bosons and $\tan\beta$ is the ratio of the two vacuum expectation values. Interpreting the LEP searches as testing the coupling of a hypothetical 98 GeV Higgs to Z bosons the observed 95% confidence level upper limit on $(g_{HZZ}/g_{HZZ}^{\mathrm{SM}})^2$ is 0.3 while the expected limit would have been 0.1 [1]. The argument can be turned around: to predict the number of events seen at LEP for a 98 GeV light-Higgs boson the coupling g_{hZZ}^2 has to be around $1/10$ of its standard model value. Following Ref. [2] we constrain $0.056 \lesssim \sin^2(\beta - \alpha) \lesssim 0.144$ at 1σ. Throughout this paper we use the same range of all Higgs sector parameters as Ref. [2] to allow for an easy comparison of the results.

Now the analogous coupling and the mass of the heavy CP-even Higgs is predicted by the MSSM-Higgs sector within the theoretical uncertainty. The coupling $g_{HZZ}^2 \propto \cos^2(\beta - \alpha) \sim 0.9$ is only slightly suppressed compared to the standard model value and is consistent with the number of events reported by LEP corresponding to a 115 GeV Higgs boson. This means we can treat both excesses as independent tests of our MSSM-Higgs hypothesis—in complete analogy to the combination of several Higgs decay signatures in the LEP analysis. Just multiplying the probabilities for background fluctuations gives us 0.18%, which is well above a 3σ excess [2]. A possible complication are ''look elsewhere'' effects, which reduce the Gaussian significance. If for illustration purpose we take an arbitrary toy value for the increase of the fluctuation probability of e.g. 5, the Gaussian significance decreases from 3.1σ to 2.6σ. However, the analyses for both mass values are optimized for the standard model Higgs hypothesis, which means that the significance for the MSSM-Higgs hypothesis can be expected to increase again.

The mass scale of the MSSM-Higgs sector is usually fixed by the mass of the pseudoscalar Higgs boson m_A. In the well-known leading m_t^4 approximation [4,5], we can very roughly link the pseudoscalar mass to the two scalar Higgs masses in the limit of nonmixing top squarks:

$$m_h^2 + m_H^2 = m_A^2 + m_Z^2 + \epsilon, \qquad m_{H^\pm}^2 = m_A^2 + m_W^2,$$
$$\epsilon = \frac{3G_F}{\sqrt{2}\pi^2} \frac{m_t^4}{\sin^2\beta} \log\frac{m_{\tilde{t}}^2}{m_t^2}. \tag{1}$$

In this approximation $m_{\tilde{t}}$ is the top squark mass, $m_{h,A,H}$ are the neutral Higgs masses and $m_{H^\pm}$ is the charged Higgs mass. We immediately see that the existence of two light scalar Higgs bosons leads to all of the MSSM-Higgs bosons being fairly light. This feature is preserved by the complete set of two-loop corrections [6] in our numerical

analysis. This can lead to interesting phenomenology in the MSSM. In this article, we consider the constraints on this scenario from the $B \to X_s\gamma$ and $B_s \to \mu^+\mu^-$ branching fractions and the magnetic moment of the muon. We discuss the implications of such a model on the phenomenology of neutralino dark matter, and find the prospects for the direct detection of neutralinos in elastic scattering experiments to be excellent. We then study the spectra of the superpartners and the Higgs sector with two light-Higgs scalars and discuss in detail the prospects for discovering the charged Higgs boson at the LHC.

In order to study the phenomenology of supersymmetric models with light-Higgs scalars, we first performed a scan over the relevant parameters of the MSSM. We have varied all masses (M_1, M_2, M_3, and all squark and slepton masses) between 0 and 6 TeV, and $\tan\beta$ (linearly) between 1 and 60. Although we varied m_A up to 1 TeV, we found no points with nearly so heavy a pseudoscalar Higgs. We did not assume any specific supersymmetry breaking scenario or unification scheme. To take into account the radiative corrections to the Higgs masses, we have used FeynHiggs [6], which includes all contributions up to the two-loop level. We find that this level of precision is needed to obtain an accurate representation of the MSSM phenomenology within this class of models. We give a detailed analysis of the Higgs sector in Sec. IV.

In Fig. 1, we confirm the conclusion of Ref. [2] that the entire MSSM-Higgs sector is required to be rather light to accommodate both excesses reported by LEP. In the overwhelming majority of models found, the mass of the pseudoscalar Higgs bosons is between 95 and 130 GeV and the mass of the charged Higgs lies between 110 and 150 GeV. Although we do find some points outside of this range, in particular, a trail of models extending to the upper right of the figure (left frame), these are less common than the dense collection of models near $m_A \sim 110$ GeV and $m_{H^\pm} \sim 130$ GeV. For each point shown, we require $95 < m_h < 101$ GeV, $111 < m_H < 119$ GeV and $0.056 \lesssim \sin^2(\beta - \alpha) \lesssim 0.144$, corresponding to the range needed to match the observations at LEP. The differences between this figure and the corresponding one in Ref. [2] come from the fact that we scan continuously over $\tan\beta$. In the right frame of Fig. 1, we check the mass of the charged Higgs boson for correlations with the value of μ. We have checked that indeed the trails of scattered points at large pseudoscalar masses correspond to the larger values of $\tan\beta$ the larger the corresponding charged Higgs masses become. Without imposing additional constraints we find relatively little correlation, for example, between the Higgs masses and the μ parameter, apart from the chargino mass limit of 104 GeV from LEP.

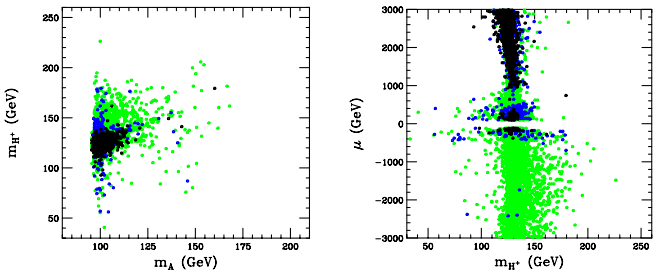

FIG. 1 (color online). The mass of the pseudoscalar Higgs versus the charged Higgs is shown in the left frame. In the right frame, μ is shown with the charged Higgs mass. For all points shown, $95 < m_h < 101$ GeV, $111 < m_H < 119$ GeV and $0.056 \lesssim \sin^2(\beta - \alpha) \lesssim 0.144$, corresponding to the range matching the observations at LEP. The black points are consistent with measurements of $B \to X_s\gamma$ at the 3σ level and do not violate the Tevatron constraint on the $B_s \to \mu^+\mu^-$ branching fraction, $\mathrm{BR}(B_s \to \mu^+\mu^-) < 5.8 \times 10^{-7}$. Dark (blue) points violate $B_s \to \mu^+\mu^-$, but are consistent with $B \to X_s\gamma$. Light (green) points violate $B \to X_s\gamma$. These constraints will be discussed further in Sec. II.

II. INDIRECT CONSTRAINTS FROM $B \to X_s\gamma$, $B_s \to \mu^+\mu^-$ AND $(g-2)_\mu$

Constraints from rare B decays and the magnetic moment of the muon are some of the most useful tools we currently have to guide our studies of supersymmetric phenomenology. The B physics constraints gain their power mostly because of a possible $\tan\beta$ enhancement of the bottom Yukawa couplings. In this section, we consider some of these constraints within the context of models with 98 and 115 GeV Higgs bosons.

The branching fraction of B decays to a strange state plus a photon has been measured by the BELLE, *BABAR*, CLEO and ALEPH experiments. The weighted average of these experiments' results indicate $\mathrm{BR}(B \to X_s\gamma) = (3.54 \pm 0.30) \times 10^{-4}$ [7]. In comparison, the standard model prediction for this transition rate is $(3.70 \pm 0.30) \times 10^{-4}$ [8].

The supersymmetric processes which are most likely to contribute substantially to this branching ratio involve a charged Higgs or a chargino. These contributions are enhanced by powers of the Yukawa coupling $m_b \tan\beta$ for large values of $\tan\beta$. In passing we emphasize that there are additional Δ_b corrections [9] which can have huge effects if the MSSM spectrum is split between light gluinos or Higgsinos and heavier sbottoms, but we will see that this is not the part of parameter space in which we are interested in. If the gluino mass is smaller than 300 GeV, the LHC will be swamped by gluino pair production with cross sections as large as 1000 pb and the effect of the gluino mass on the charged Higgs boson is negligible.

Assuming minimal flavor violation throughout this paper we plot $\mathrm{BR}(B \to X_s\gamma)$ versus $\tan\beta$ (upper left frame), the lightest chargino mass (bottom center frame) and the charged Higgs mass (upper right frame) in Fig. 2. Shown as horizontal dashed lines are the 2σ confidence bounds on this branching fraction. Again, all points shown have $95 < m_h < 101$ GeV, $111 < m_H < 119$ GeV and

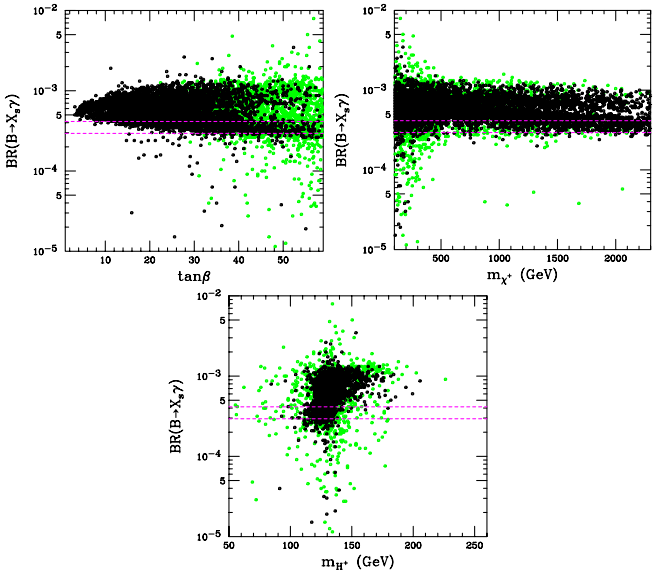

FIG. 2 (color online). The $b \to s\gamma$ branching fraction as a function of $\tan\beta$, the lightest chargino mass, and the charged Higgs mass. Shown as horizontal dashed lines are the 2σ confidence bounds on this quantity as measured by BELLE, *BABAR*, CLEO and ALEPH. Again, all points shown have $95 < m_h < 101$ GeV, $111 < m_H < 119$ GeV and $0.056 \lesssim \sin^2(\beta - \alpha) \lesssim 0.144$. Black points do not violate the Tevatron constraint on the $B_s \to \mu^+\mu^-$ branching fraction, $\mathrm{BR}(B_s \to \mu^+\mu^-) < 5.8 \times 10^{-7}$. Light (green) points violate this constraint.

$0.056 \lesssim \sin^2(\beta - \alpha) \lesssim 0.144$. Strictly applying a 2σ limit would rule out all points with $\tan\beta \lesssim 10$, but on the other hand allowing for a 3σ deviation from the standard model brings all values of $\tan\beta$ back into the allowed region. Note that the preference of larger values of $\tan\beta$ is due to a slight bias toward a finite MSSM contribution: if we force the Higgs sector to be light, the two Higgs doublet model (2HDM) diagrams will lead to an increase of the observable $\mathrm{BR}(B \to X_s\gamma)$ by typically tens of percent up to a factor of 2. These charged Higgs contributions consist of a $\tan\beta$ suppressed term and a constant term, but do not exhibit any $\tan\beta$ enhancement (if we do not consider anomalously large gluino loops). Because the measured value of $\mathrm{BR}(B \to X_s\gamma)$ is actually slightly smaller than the standard model prediction, the chargino has to compensate for the 2HDM contribution. Because the chargino contribution to $\mathrm{BR}(B \to X_s\gamma)$ is enhanced by one power of $\tan\beta$ on the amplitude level, we can achieve this by choosing large values of $\tan\beta$, as we see in the left panel of Fig. 2. We can, of course, try to increase the chargino diagram by making the chargino light, but this is much less efficient, because the loop involved is a chargino-stop loop, so that just making the chargino light has comparably little effect. Again, we see in the bottom center frame of Fig. 2 that very light chargino masses serve this purpose. Moreover, the large chargino contribution has to come with the right sign and therefore prefers positive μ, as shown in Fig. 1. As we can see, the charged Higgs mass and therefore the contribution to $\mathrm{BR}(B \to X_s\gamma)$ is basically fixed by the two light-Higgs masses. Thus merely shifting the charged Higgs mass between 120 and 170 GeV has even less of an effect.

Limits on the branching fraction of the rare decay $B_s \to \mu^+\mu^-$ can also be exploited to limit the allowed MSSM parameter space. The standard model prediction for this branching ratio is $\mathrm{BR} = (3.4 \pm 0.5) \times 10^{-9}$ [10]. In particular, the Higgs-induced MSSM contribution to this branching fraction scales with $\tan^6\beta/m_A^4$ and tends to be especially large in our scenario with a light-Higgs sector [11]. If we require the Higgs sector to be light, models with very large values of $\tan\beta$ are likely to violate the constraints on this quantity placed at the Tevatron [12]. In Fig. 3, we plot $\mathrm{BR}(B_s \to \mu^+\mu^-)$ versus $\tan\beta$. Shown as a dashed horizontal line is the 90% upper confidence bound placed by the Tevatron experiments. The standard model value is clearly visible as the low $\tan\beta$ nose in the distribution of the MSSM parameter points—small $\tan\beta$

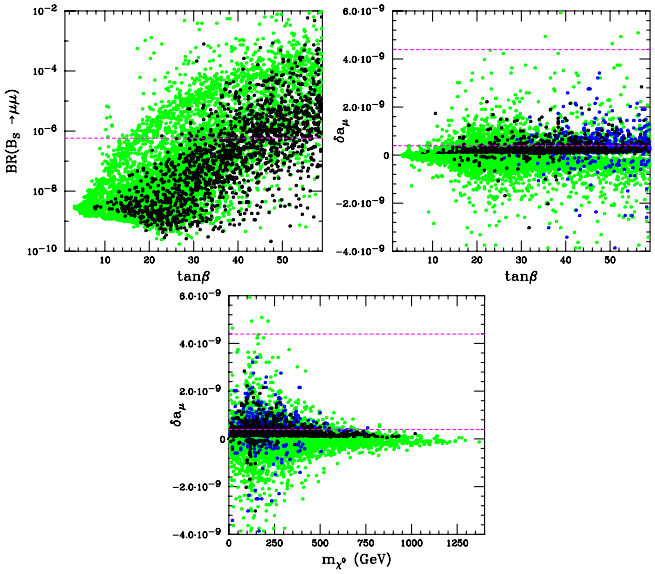

FIG. 3 (color online). (Left panel) The $B_s \to \mu^+\mu^-$ branching fraction versus $\tan\beta$. The dashed horizontal line is the 90% upper confidence bound placed on this branching fraction by the Tevatron experiments, $\mathrm{BR}(B_s \to \mu^+\mu^-) < 5.8 \times 10^{-7}$. Black points are consistent with measurements of $B \to X_s\gamma$ at the 3σ level. Light (green) points violate this constraint. (Upper right, bottom center panels) The contribution to the magnetic moment of the muon. The dashed horizontal lines are the 2σ bounds from e^+e^- data. The black points are consistent with measurements of $B \to X_s\gamma$ at the 3σ level and do not violate the Tevatron constraint on the $B_s \to \mu^+\mu^-$ branching fraction, $\mathrm{BR}(B_s \to \mu^+\mu^-) < 5.8 \times 10^{-7}$. Dark (blue) points do violate $B_s \to \mu^+\mu^-$, but are consistent with $B \to X_s\gamma$. Light (green) points violate $B \to X_s\gamma$. All points shown have $95 < m_h < 101$ GeV, $111 < m_H < 119$ GeV and $0.056 \lesssim \sin^2(\beta - \alpha) \lesssim 0.144$.

means small contributions from the MSSM-Higgs sector. The upper limit from the Tevatron becomes an issue for $\tan\beta > 10$ but it really only develops seriously destructive power for $\tan\beta > 50$.

Combining the upper limit on the $B_s \to \mu^+\mu^-$ decay and the measurement of $B \to s\gamma$ makes it considerably harder for us to find viable MSSM scenarios with two light-Higgs scalars. On the one hand, we need an MSSM contribution to $B \to X_s\gamma$ from the chargino sector with the right sign and magnitude to compensate for the charged Higgs diagrams. This is possible by exploiting the enhancement by one power of $\tan\beta$ in the chargino amplitude. On the other hand, we do not want too large a contribution to $B_s \to \mu^+\mu^-$ from the same sector which scales as $\tan^6\beta$. Putting both of these constraints together, we favor fairly large, but not too large, values of $\tan\beta$ and at the same time accept some light superpartners to accommodate $B \to X_s\gamma$. We should stress, however, that this argument is not strict in the sense that these two constraints guarantee a light MSSM mass spectrum. By choosing properly tuned parameters, we can still get by with a spectrum where the lightest of the charginos and stops weighs more than 1 TeV.

Looking into the near future, we see that of course the LHC prospects of seeing these light-Higgs MSSM scenarios in B physics are excellent. Simulations of CMS, ATLAS and LHCb events probing $\mathrm{BR}(B_s \to \mu^+\mu^-)$ predict tens of events for 10 fb^{-1} and the standard model decay rate. Moreover, it has been shown that high luminosity triggering on this search channel is possible, so that the LHC reach should even cover smaller branching fractions than predicted in the standard model. Basically all parameter points shown in Fig. 3 will be clearly visible [13]. The only question is whether the theoretical and experimental errors will allow us to distinguish between the standard model and the MSSM predictions.

Finally, the magnetic moment of the muon has been measured to be anomalously high in comparison to the standard model prediction. Using e^+e^- data, the measured value exceeds the theoretical prediction by $\delta a_\mu(e^+e^-) = 23.9 \pm 7.2_{\text{had-lo}} \pm 3.5_{\text{lbl}} \pm 6_{\text{exp}} \times 10^{-10}$, where the error bars correspond to theoretical uncertainties in the leading order hadronic and the hadronic light-by-light contributions as well as from experimental contributions [14,15]. This measured value is 2.4σ above the standard model prediction. Experiments using τ data, on the other hand, find $\delta a_\mu(\tau^+\tau^-) = 7.6 \pm 5.8_{\text{had-lo}} \pm 3.5_{\text{lbl}} \pm 6_{\text{exp}} \times 10^{-10}$, which is only 0.9σ above the standard model prediction and likely not in agreement with the most recent KLOE data [16]. Given this conflict and the marginal statistical significance of these measurements, we do not require all of our scenarios to produce the measured value of $(g-2)_\mu$.

Contributions to $(g-2)_\mu$ occur at the one- and two-loop levels from diagrams involving both Higgs bosons [17] and superpartners [18]. At the one-loop level the contribution from superpartner exchange is proportional to $a_\mu^{\text{SUSY}} \propto \tan\beta/m_{\text{SUSY}}\,\text{sgn}(\mu)$ [18]. The exchange of a light pseudoscalar Higgs contributes like $a_\mu^{\text{2HDM}} \propto \tan^2\beta/m_A^2$ in the leading order of $\tan\beta$. Because we are only considering models with a light-Higgs sector, the effects from the A exchange will dominate. This is what we see in the $\tan\beta$ dependence of the permitted parameters points in Fig. 3. In a way, the situation is the same as for $B \to X_s\gamma$: both measurements sit very slightly away from their respective standard model predictions (and from a statistical point of view are not very convincing), and the central values can be accommodated by choosing large $\tan\beta$. In the upper right and center bottom panels of Fig. 3 we see that the $B \to X_s\gamma$ constraint goes a long way to also accommodate the $(g-2)_\mu$ measurement in our MSSM parameter space. This is particularly striking when we look at the behavior of the points around $\delta a_\mu = 0$. The $B \to X_s\gamma$ constraint disfavors the ''wrong'' sign of δa_μ already, so that the impact of the $(g-2)_\mu$ measurement on our light-Higgs models is very limited once we allow slightly more than a 2σ window. Again, we see how very large values of $\tan\beta$ are disfavored by $B_s \to \mu^+\mu^-$, which drives the MSSM parameter points toward lighter superpartners, i.e. lighter stops and charginos/neutralinos. This constraint is expected to become more stringent over the coming years, even before the LHC will start operation.

To calculate $\mathrm{BR}(B \to X_s\gamma)$, $\mathrm{BR}(B_s \to \mu^+\mu^-)$ and δa_μ, we have used the MICROMEGAS program [19].

III. IMPLICATIONS FOR NEUTRALINO DARK MATTER

One very attractive feature of R-parity conserving supersymmetry is that it naturally provides a stable particle which, in many models, can be a viable candidate for dark matter. The lightest neutralino is particularly appealing in this respect [20].

Neutralinos can annihilate through a variety of channels, including through the exchange of CP-even or -odd Higgs bosons, charginos, neutralinos, sfermions and gauge bosons. Which annihilation channel(s) dominates varies from model to model. In the scenario we are studying here, however, the presence of light-Higgs bosons suggest that s-channel Higgs exchange to fermion pairs is likely to be a particularly efficient annihilation channel, especially in those models with moderate to large values of $\tan\beta$. The formulas for these annihilation channels are collected in the Appendix.

The annihilation cross section can be used to calculate the thermal relic abundance present today:

$$\Omega_{\chi^0}h^2 \approx \frac{10^9}{M_{\text{Pl}}}\frac{x_{\text{FO}}}{\sqrt{g_\star}}\frac{1}{(a+3b/x_{\text{FO}})}, \tag{2}$$

where $g_\star$ is the number of relativistic degrees of freedom

available at freeze-out, a and b are the amplitudes given in the Appendix, and $x_{\rm FO}$ is the value at freeze-out, which can be found by solving:

$$x_{\rm FO} \approx \ln\left(\sqrt{\frac{45}{8}}\frac{m_{\chi^0} M_{\rm Pl}(a+6b/x_{\rm FO})}{\pi^3\sqrt{g_\star x_{\rm FO}}}\right). \quad (3)$$

Over the range of cross sections and masses expected for the lightest neutralino, $x_{\rm FO} \approx 20$–30. To yield the density of cold dark matter measured by WMAP [21], we thus require $a + 3b/x_{\rm FO} \approx 3 \times 10^{-26}$ cm^3/s. The main contributions to a and b are s-channel CP-odd and CP-even Higgs exchanges, respectively. From the amplitudes given in the Appendix, we find $a \sim b \times \tan^2\beta/3$, so we conclude that the b term induced through CP-even Higgs plays a subdominant role in the relic density calculation to the CP-odd Higgs-induced a term. In the left frame of Fig. 4, we plot the relic density of the lightest neutralino versus its mass. We have calculated this quantity using the MICROMEGAS program [19].

Over the vast majority of supersymmetric parameter space, the composition of the lightest neutralino is dominated by its b-ino component, although a small admixture of W-ino or Higgsino is common. For a b-ino-like neutralino with large or moderate $\tan\beta$, the annihilation cross section through pseudoscalar Higgs exchange scales as $\epsilon_u^2 \tan^2\beta$. The up-type Higgsino component can be approximated in most models by $\epsilon_u^2 \approx \epsilon_B^2 \sin^2\theta_W \sin^2\beta m_Z^2/\mu^2$, where ϵ_B^2 is the b-ino component of the lightest supersymmetric particle (LSP). With this in mind we plot the neutralino relic density versus the quantity $\tan^2\beta \sin^2\theta_W m_Z^2/\mu^2$ in the right frame of Fig. 4. The two solid lines shown are the analytic results for $m_A = 120$ GeV and $m_{\chi^0} = 50$ (bottom) and 500 (top) GeV in this approximation. The majority of models we find fall within this range, suggesting that their annihilation is in fact dominated by an s-channel pseudoscalar Higgs exchange to $b\bar{b}$. As expected, no models fall above this range. In the models which lie below this range, another annihilation mode or modes (such as t-channel sfermion exchange, s-channel Z exchange or s-channel pseudoscalar Higgs exchange to top quark pairs) must contribute substantially, thus lowering the relic abundance accordingly. Coannihilations between the lightest neutralino and another superpartner may also reduce the relic density.

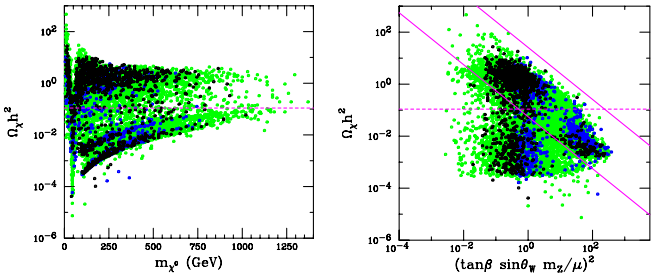

FIG. 4 (color online). The thermal relic abundance of neutralino dark matter. The dashed horizontal line represents the density measured by WMAP [21]. In the right frame, we compare the relic density to the quantity $\tan^2\beta \sin^2\theta_W m_Z^2/\mu^2$, which for models with a b-ino-like lightest neutralino is a good approximation for $\epsilon_u^2 \tan^2\beta$, and therefore scales with the annihilation cross section to $b\bar{b}$ via pseudoscalar Higgs exchange. The two solid lines represent the analytic result of this calculation using $m_A = 120$ GeV and $m_{\chi^0} = 50$ (bottom) and 500 (top) GeV. All models shown have $95 < m_h < 101$ GeV, $111 < m_H < 119$ GeV and $0.056 \lesssim \sin^2(\beta-\alpha) \lesssim 0.144$. The black points are consistent with measurements of $B \to X_s\gamma$ at the 3σ level and do not violate the Tevatron constraint on the $B_s \to \mu^+\mu^-$ branching fraction. Dark (blue) points violate $B_s \to \mu^+\mu^-$, but are consistent with $B \to X_s\gamma$. Light (green) points violate $B \to X_s\gamma$.

From the right frame of Fig. 4, we can infer that for those models which generate the measured relic abundance (those which fall along the horizontal dashed line), most appear to annihilate substantially through pseudoscalar Higgs exchange to $b\bar{b}$. Models with a b-ino-like neutralino with a small Higgsino admixture and moderate to high value of $\tan\beta$ are often capable of generating the measured density of dark matter.

The prospects for the direct detection of particle dark matter are quite encouraging for a neutralino in conjunction with a light-Higgs sector. In many of the models we study here, the spin-independent neutralino-nucleon elastic scattering cross section is dominated by the t-channel exchange of CP-even Higgs bosons. The cross section for this process is roughly given by

$$\sigma_{\chi N} \approx \frac{8G_F^2 m_Z^2}{\pi m_H^4}\left(\frac{m_p m_{\chi^0}}{m_p + m_{\chi^0}}\right)^2 (-\epsilon_B \sin\theta_W + \epsilon_W \cos\theta_W)^2 \times \epsilon_H^2\left[\sum_q \frac{m_q}{\cos\beta}\langle N|q\bar{q}|N\rangle\right]^2, \quad (4)$$

where the sum is over quark types and $\langle N|q\bar{q}|N\rangle$ are the matrix elements over the nucleonic state. The quantity $\cos\beta$ should be replaced with $\sin\beta$ for up-type quarks. ϵ_B^2, ϵ_W^2 and ϵ_H^2 are the b-ino, W-ino and Higgsino fractions of the neutralino. In the sum over quark species, the strange quark contribution dominates with $m_s\langle N|s\bar{s}|N\rangle \approx 0.2$ GeV. For models with $\sim$100 GeV Higgs bosons and a b-ino-like LSP, we estimate

$$\sigma_{\chi N} \sim 10^{-7}\text{–}10^{-6}\ \text{pb}\left(\frac{\epsilon_H^2}{0.01}\right)\left(\frac{\tan\beta}{20}\right)^2. \quad (5)$$

Of course other elastic scattering channels (squark exchange, in particular) can also contribute substantially. In Fig. 5 we show the spin-independent neutralino-nucleon elastic scattering cross section for models in this scenario. Models shown in the right frame each generate an abundance of neutralino dark matter within 1 order of magnitude of the observed density, while those models shown in

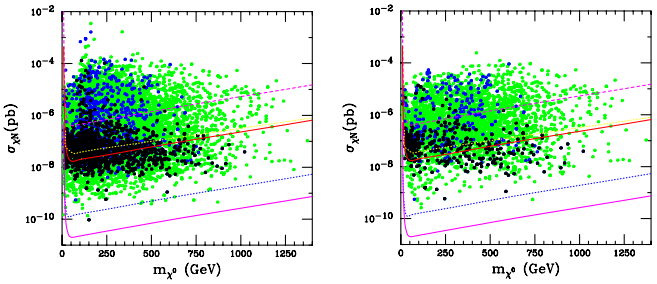

FIG. 5 (color online). The spin-independent neutralino-nucleon elastic scattering cross section is shown versus the neutralino mass. All points shown have $95 < m_h < 101$ GeV, $111 < m_H < 119$ GeV and $0.056 \lesssim \sin^2(\beta - \alpha) \lesssim 0.144$. The left frame includes models with any relic density, while those models shown in the right frame generate an abundance of dark matter within a factor of 10 of the observed quantity. The dashed curve in each frame is the current limit placed by the CDMS experiment. The light dotted (yellow), dark solid (red), light dotted (blue) and dark solid (magenta) curves (from top to bottom) are the approximate projected limits of GERDA, CDMS, ZEPLIN-MAX and Super-CDMS (phase III), respectively. The black points are consistent with measurements of $B \to X_s\gamma$ at the 3σ level and do not violate the Tevatron constraint on the $B_s \to \mu^+\mu^-$ branching fraction. Dark (blue) points violate $B_s \to \mu^+\mu^-$, but are consistent with $B \to X_s\gamma$. Light (green) points violate $B \to X_s\gamma$.

the left frame may or may not. The dashed curve in each frame is the current limit placed by the CDMS II experiment [22]. The light dotted (yellow), dark solid (red), light dotted (blue) and dark solid (magenta) curves (from top to bottom) are the approximate projected limits of the GERDA [23], CDMS II, ZEPLIN-MAX [24] and Super-CDMS (phase III) experiments, respectively. Edelweiss [25] should also reach a sensitivity similar to that of CDMS. To calculate these elastic scattering cross sections, we have used the DARKSUSY program [26].

From Fig. 5, it is obvious that the prospects for direct detection are excellent for this class of supersymmetric models with light-Higgs sectors which often dominate the cross section. Most of the favored models are within the reach of the CDMS and Edelweiss experiments and those remaining models below this level of sensitivity should be within the reach of next generation experiments such as ZEPLIN-MAX or Super-CDMS.

It is straightforward to understand why models with very small elastic scattering cross sections do not appear in Fig. 5. If we limit the magnitude of μ to be less than a few TeV for fine-tuning reasons, the Higgsino fraction of the lightest neutralino is then bounded from below to be $\epsilon_u^2 \gtrsim \sin^2\theta_W \sin^2\beta m_Z^2/(3\ \text{TeV})^2 \sim 0.0002$. From this, we see that $\sigma_{\chi N}$ cannot be smaller than 10^{-9} to 10^{-10} pb without $|\mu|$ being unnaturally large.

In addition to these excellent prospects for direct dark matter searches, the characteristics of the lightest neutralino in this class of models are fairly ideal for the purposes of indirect detection. Since the annihilation cross section during freeze-out is dominated by the first term in the expansion, $\langle\sigma v\rangle = a + bx + \mathcal{O}(x^2)$, the annihilation cross section relevant for neutralinos annihilating near the galactic center, throughout the galactic halo, or elsewhere of interest to indirect detection, is the maximum value consistent with the measured relic abundance, $\langle\sigma v\rangle \approx 3 \times 10^{-26}$ cm^3/s. This makes it rather likely that such models will be within the reach of future indirect detection experiments searching for neutralino annihilation products in the form of gamma rays [27] or antimatter [28]. The prospects for detecting such a neutralino in future cosmic positron experiments are especially promising.

IV. LIGHT MSSM-HIGGS BOSONS AT THE LHC

Before we begin discussing the prospects of observing a light MSSM-Higgs sector at the LHC, we should point out that it has been known for a long time that one CP-even Higgs scalar in the MSSM is guaranteed to be seen in weak-boson-fusion production with a subsequent decay $h,\ H \to \tau\tau$ [29]. The search strategy is identical to the standard model search for low Higgs masses and has been extensively studied including detector effects [30]. In the special case of three light MSSM-Higgs scalars, this discovery channel is known to face a challenge: the $\tau\tau$ mass resolution will not be sufficient to resolve the two CP-even scalars if their mass difference is less than $\mathcal{O}(5)$ GeV—they will appear as one sightly wider Higgs resonance. Moreover, the pseudoscalar Higgs only couples to gauge bosons through a dimension-5 operator [31], thus it will not be produced in weak-boson fusion. The case of three almost mass-degenerate light-Higgs scalars has been specifically studied, with an emphasis on distinguishing the three mass peaks in the decay to muons [32]. The conclusion is that for Higgs masses below 140 GeV, the inclusive Higgs search is challenging and that the heavy Higgs bosons will probably not be separately observable in this channel. The more promising strategy is to look for bottom-Higgs associated production with a subsequent Higgs decay to muons and at least one b tag. The Yukawa coupling for the heavy scalar and the pseudoscalar Higgs can then be $\tan\beta$ enhanced and the mass peaks might be resolved for $\tan\beta \gtrsim 30$ and $m_A \gtrsim 130$ GeV.

The general lesson we learn from detailed studies by ATLAS and CMS is that it might well be easier to discover a charged Higgs boson than the additional neutral scalars. A charged Higgs can be searched for either in anomalous top decays, or it can be directly produced as $bg \to tH^-$. In both cases the decay to a tau lepton is most promising [33]. The coverage of models in the (m_A-$\tan\beta$) plane from this channel has historically included a hole for charged Higgs masses just above the top mass. We emphasize that this hole does not mean that the charged Higgs will be missed at the LHC in this parameter range. It just means that we will have to combine the search strategies for (off-shell)

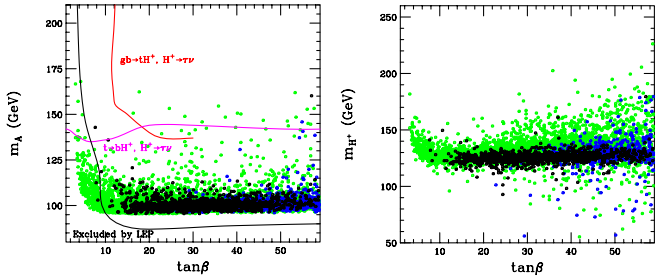

FIG. 6 (color online). (Left panel) The (5σ, 300 fb^{-1}) discovery potential for a charged Higgs boson at the LHC. Below the nearly horizontal (middle, magenta) line, charged Higgs bosons can be identified through the $t \to H^\pm b$, $H^\pm \to \tau\nu$ channel. Models falling to the upper right of the top (red) line can be discovered through the channel $bg \to tH^\pm$, $H^\pm \to \tau\nu$. Models with very light A, $H^\pm$ or very small $\tan\beta$ are excluded by LEP. (Right panel) The same points shown in the $m_{H^\pm}$ vs $\tan\beta$ plane. All models shown have $95 < m_h < 101$ GeV, $111 < m_H < 119$ GeV and $0.056 \lesssim \sin^2(\beta - \alpha) \lesssim 0.144$. The black points are consistent with measurements of $B \to X_s\gamma$ at the 3σ level and do not violate the Tevatron constraint on the $B_s \to \mu^+\mu^-$ branching fraction. Dark (blue) points violate $B_s \to \mu^+\mu^-$, but are consistent with $B \to X_s\gamma$. Light (green) points violate $B \to X_s\gamma$.

anomalous top decays with the usual associated production [34]. For the purpose of this paper we will use a preliminary parton level analysis [35]. We include this result in Fig. 6.

A. Light charged Higgs bosons

Phenomenologically speaking, the easiest searches for charged Higgs bosons are in the mass range $m_{H^\pm} \lesssim m_t - m_b$. A light charged Higgs will almost exclusively decay to a tau lepton, because the decay to $t\bar{b}$ is kinematically closed in our scenario. As long as the charged Higgs is lighter than the top we would not expect the decay to Wh^0 to lead to a sizable branching either. This might change once the charged Higgs mass is above the top threshold. This means we can look for top decays to $b\ell\bar{\nu}$, where there are too many final state taus as compared to muons and electrons. In top pair production we let the second top decay into Wb, where the W can decay leptonically and hadronically (the latter channel dominates the reach in the charged Higgs mass) [36]. The tau from the charged Higgs typically forms a jet. The partial width of a top decay to a charged Higgs contains two terms: $m_b^2 \tan^2\beta + m_t^2/\tan^2\beta$. Hence, there will be large branching fractions both for small and large values of $\tan\beta$ with the weakest point around $\tan\beta \sim \sqrt{m_t/m_b} \sim 7$. Because at the LHC these searches are sensitive to anomalous branching fractions of the order of 1% [37], we can expect them to probe charged Higgs masses up to $m_{H^\pm} \lesssim m_t - m_b \sim 160$ GeV. Including off-shell effects, this reach might even be extended by a few GeV. At the Tevatron the same searches are currently in progress, but are strongly statistics limited [38]. They only cover anomalous branching fractions of the order of 60%, corresponding to an enhanced Yukawa coupling $\tan\beta \gtrsim 20$ and masses $m_{H^\pm} \lesssim 140$ GeV.

In Fig. 6 we overlay our MSSM parameter points with the approximate LHC (ATLAS) 5σ reach. The discovery contours in the left panel of Fig. 6 are of course based on a specific MSSM-Higgs scenario. Therefore, we only use this overlay to illustrate the three parameter regions with different consequences for LHC searches discussed in this section. The right panel in Fig. 6 shows the parameters which actually determine the phenomenology of charged Higgs bosons at the LHC. The middle (magenta) line in the left panel corresponds to the low-luminosity results from anomalous top decays. The slight bending comes from the mass relation between m_A and $m_{H^\pm}$ as well as from the coupling suppression for intermediate $\tan\beta$. We see that most of the parameter points with two light-Higgs scalars will be clearly visible in anomalous top decays at the LHC, possibly even at the Tevatron.

B. Heavy charged Higgs bosons with large $\tan\beta$

The best-studied regime for charged Higgs searches at the LHC is the region of large $\tan\beta \gtrsim 10$ and charged Higgs masses well above the top threshold. Following the approximation in Eq. (1), we see that the required two light scalar Higgs bosons imply $\sqrt{m_A^2 + m_Z^2 + \epsilon} \sim 150$ GeV. Requiring charged Higgs masses above the top threshold translates into $m_A > 150$ GeV, or in other words $m_Z^2 \sim -\epsilon$. This could be possible if one stop were much lighter than the top. On the other hand, the ϵ approximation is based on the assumption of nonmixing stops, so we postpone this light-stop scenario to the next subsection. The other way of enhancing the mass difference between the average CP-even Higgs mass and the charged Higgs mass (beyond the simple m_t^4 approximation) and to escape the anomalous top decays is to create large bottom Yukawa corrections through large values of $\tan\beta$ (while keeping the μ parameter small). This leads to additional terms contributing to the charged Higgs mass squared, the leading terms of which are proportional to $m_t^2 m_b^2$. The two kinds of contributions which appear with this mixed Yukawa coupling are either proportional to $\log(m_{\tilde{t}_1} m_{\tilde{t}_2}/m_t^2)$, or they come without this logarithm and are directly proportional to the average stop mass instead [5]. We see their effect in Fig. 6 when we compare the $\tan\beta$ dependence of m_A and $m_{H^\pm}$. For all values of $\tan\beta$ the requirement of two light-Higgs scalars limits the pseudoscalar mass to a narrow corridor. We find hardly any SUSY scenarios with $m_A > 110$ GeV. By considering large values of $\tan\beta$, we can increase the charged Higgs mass by 50 GeV and avoid the top decay threshold.

Because large values of $\tan\beta$ are required at the same time to have two light-Higgs scalars and a heavier charged

Higgs, we are automatically driven into the region where the charged Higgs can be found in tH^- production at the LHC. The only issue is the hole which usually appears in the LHC coverage region for charged Higgs masses between 160 and 200 GeV. As mentioned above, this hole is an artifact of the two search strategies meeting in this mass range. The associated production process and the anomalous (off-shell) top decay have to be combined to cover this hole. This kind of study is ongoing in CMS and in ATLAS [35] and we do not expect this to be a problem once these analyses are actually performed on data. In Fig. 6 the densities of points suggests that it might be very unlikely to find such a light-Higgs MSSM scenario where the LHC sees only one neutral Higgs scalar and no charged Higgs (we find only one point somewhat close to this region in our scan). However, because the region is not excluded, we will study these kinds of parameter points and their discovery prospects at the LHC in more detail next, to ensure there is no hole in the LHC discovery range.

C. Heavy charged Higgs bosons and light stops

As described above, there is this remaining part of the light-scalars parameter space where charged Higgs searches in anomalous top decays and in the associated production with a top are challenging. It requires charged Higgs masses just above the top threshold and small $\tan\beta$. Note that we do not claim that LHC will not see a charged Higgs in this region of parameter space. Instead, we emphasize that covering this hole is a crucial task for the near future. To study this region of parameter space in more detail we perform a dedicated scan around one point which appears in Fig. 6 close to the hole in the LHC reach for intermediate $\tan\beta < 20$ and $m_{H^\pm} \sim 180$ GeV. We vary each mass parameter up to 50% above or below the value of the single point at $\tan\beta \approx 8$, $m_A \approx 140$ shown in Fig. 6. Only $\tan\beta$ we vary over the entire range 1–60. At this specific point, M_2 and M_3 are both $\sim$1 TeV, $\mu \sim 2$ TeV, $A_t \sim -500$ GeV, and the b-ino mass is somewhat light, $M_1 \approx 140$ GeV.

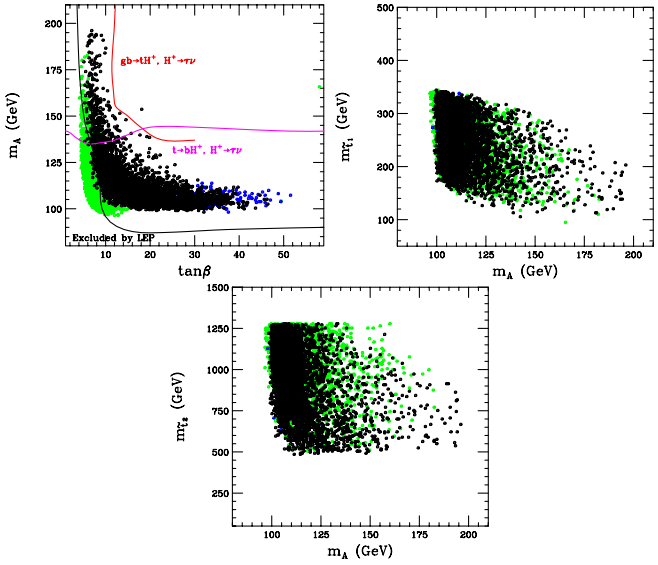

FIG. 7 (color online). (Upper left panel) Same as in Fig. 6, but with parameters varied as described in the text of Sec. IV C. (Upper right, bottom center panels) The light-stop masses for the same set of parameter points. All models shown have $95 < m_h < 101$ GeV, $111 < m_H < 119$ GeV and $0.056 \lesssim \sin^2(\beta - \alpha) \lesssim 0.144$. The black points are consistent with measurements of $B \to X_s\gamma$ at the 3σ level and do not violate the Tevatron constraint on the $B_s \to \mu^+\mu^-$ branching fraction. Dark (blue) points violate $B_s \to \mu^+\mu^-$, but are consistent with $B \to X_s\gamma$. Light (green) points violate $B \to X_s\gamma$.

To see what kind of MSSM parameter choice can enhance the charged Higgs mass compared to the CP-even scalar masses, we extend the analytical approximation of Eq. (1) to mixing stops [5]. To avoid the LHC limits, we are now interested in parameter points with as small as possible $\tan\beta$, so we can neglect the bottom Yukawa coupling. Instead, we take into account large stop mixing. In two cases the expressions are particularly simple (and in this limit of large stop mixing independent of the leading logarithm $\log m_{\tilde{t}}/m_t$):

$$\begin{aligned} m_{H^\pm}^2 - (m_h^2 + m_H^2) &= m_W^2 - m_Z^2 + \frac{G_F m_t^4}{4\sqrt{2}\pi^2} \frac{A_t^2(A_t^2+\mu^2)}{m_{\tilde{t}_1}^2 m_{\tilde{t}_2}^2}, \qquad (\tan b \to 1), \\ m_{H^\pm}^2 - (m_h^2 + m_H^2) &= m_W^2 - m_Z^2 + \frac{G_F m_t^4}{2\sqrt{2}\pi^2} \frac{(A_t-\mu)^2(A_t^2+\mu^2)}{m_{\tilde{t}_1}^2 m_{\tilde{t}_2}^2}, \qquad (\tan b \gg 1). \end{aligned} \tag{6}$$

These results point at another way of increasing the charged Higgs mass while keeping two light-Higgs scalars: we choose fairly light stops and increase the trilinear coupling, A_t, or the μ parameter. We have checked explicitly that for large values of $\tan\beta$ the same can be achieved through increasing A_b. However, keeping both stops light and at the same time increasing one way or another the stop mixing parameters, $A_t - \mu/\tan\beta$, means that at least the lighter stop and the lighter sbottom will be very light. This is precisely what we observe in Fig. 7: when we include the complete two-loop corrections in the Higgs sector [6], the lightest stop mass is always lighter than approximately 340 GeV.

Depending on the neutralino and chargino masses there are two possible stop decays we have to consider when we search for light stops at the Tevatron and at the LHC. If the stop is heavier than the lightest chargino, it will decay mostly into $b\tilde{\chi}_1^+$. If this decay channel is kinematically forbidden, as the LEP2 limits suggest for the run I stop searches at the Tevatron, the stop has to decay to $q\tilde{\chi}_1^0$.

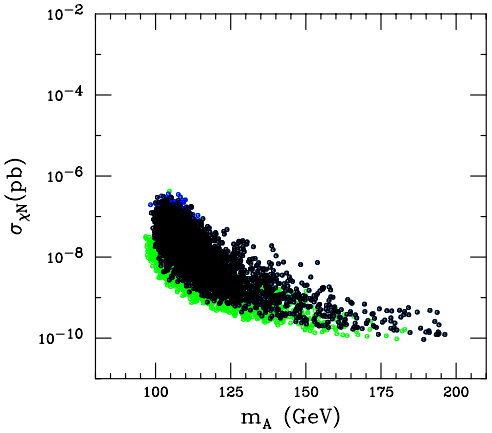

FIG. 8 (color online). The spin-independent neutralino-nucleon elastic scattering cross section is shown versus the CP-odd Higgs mass for the range of models described in Sec. IV C of the text. For those models in which charged Higgs searches at the LHC will be difficult at the LHC ($m_A \gtrsim 140$ GeV), this cross section is rather small, $\sigma_{\chi N} \sim 10^{-9}$–$10^{-10}$ pb. These models each contain a rather light neutralino, however, $m_{\chi^0} \approx 70$–200 GeV, making most of them accessible to ZEPLIN-MAX and all of them accessible to Super-CDMS (see Fig. 5). All models shown have $95 < m_h < 101$ GeV, $111 < m_H < 119$ GeV and $0.056 \lesssim \sin^2(\beta - \alpha) \lesssim 0.144$. The black points are consistent with measurements of $B \to X_s\gamma$ at the 3σ level and do not violate the Tevatron constraint on the $B_s \to \mu^+\mu^-$ branching fraction. Dark (blue) points violate $B_s \to \mu^+\mu^-$, but are consistent with $B \to X_s\gamma$. Light (green) points violate $B \to X_s\gamma$.

The production cross sections for light stops are large: at the Tevatron, a 200 GeV stop will be produced with a total cross section of approximately 300 fb, and at the LHC a 300 GeV stop will have a production rate around 10 pb. This means that at the LHC, although this kind of MSSM parameter point might be hard to find a charged Higgs boson, there will be huge numbers of top squarks establishing supersymmetry. Ongoing Tevatron searches with a projected run II reach of well above 200 GeV (dependent on the neutralino and chargino masses) will already severely constrain models with light stops.

One might worry that in these models with lower $\tan\beta$ direct dark matter detection might be more difficult. In Fig. 8 we show that this is in fact the case, with spin-independent elastic scattering cross sections as low as 10^{-10} pb. In each of these models, however, there is a rather light neutralino, $m_{\chi^0} \lesssim 200$ GeV, which makes all of these models observable by Super-CDMS and many of them observable by ZEPLIN-MAX, even for $\sigma_{\chi N} \approx 10^{-10}$ pb (see Fig. 5).

V. CONCLUSIONS

In this article, we describe the phenomenology of models within the MSSM containing CP-even Higgs bosons with masses of approximately 98 and 114 GeV, motivated by the excesses observed by LEP [2]. We study in detail indirect constraints on such light-Higgs models, coming from $B \to X_s\gamma$, $(g-2)_\mu$ and $B_s \to \mu\mu$. The first two constraints require fairly large $\tan\beta$ when compared with data, the latter tends to disfavor this regime, and the upcoming Tevatron run II results are going to close in on our light-Higgs parameter space. However, it is possible to avoid all indirect constraints by tuning the different weak-scale SUSY breaking parameters.

We find that the kind of models we are interested in typically include a light charged Higgs boson along with the other light-Higgs bosons. Such a state is observable in anomalous top decays at the Tevatron or at the LHC. Scenarios with charged Higgs above the top threshold are automatically driven in the larger $\tan\beta$ regime, where the charged Higgs can be detected in bottom-gluon fusion at the LHC. We find exceptional models which fall between these two mass regions, so that neither of the two searches is optimized and a combination of the two search tactics would be needed. However, these challenging scenarios require one very light top squark ($m_{\tilde{t}_1} \lesssim 300$ GeV), so a large fraction of them will already be ruled out at the Tevatron.

We also explore the phenomenology for neutralino dark matter in this class of models. The prospects for direct detection are excellent, with the majority of models within this scenario being testable in currently operating experiments, such as CDMS-II. We find that *all* models within this class will be testable in next generation direct dark matter detection experiments, such as ZEPLIN-MAX or Super-CDMS. The prospects for indirect are also favorable in this scenario.

ACKNOWLEDGMENTS

We would like to thank Professor Gudrun Hiller for discussing in detail the indirect constraints from B physics and for being of great help. We would also like to thank Thomas Hahn and Sven Heinemeyer for their help with FeynHiggs and Manuel Drees for valuable discussions. We are particularly grateful to Kyle Cranmer for his advice on the LEP Higgs searches and on statistics. D. H. is supported by the Leverhulme Trust.

APPENDIX: NEUTRALINO ANNIHILATION CROSS SECTIONS

The squared amplitudes for the processes, $\chi^0\chi^0 \to A \to f\bar{f}$ and $\chi^0\chi^0 \to H \to f\bar{f}$, averaged over the final state angle are given by [39]

$$\omega^A_{f\bar{f}} = \frac{C^2_{ffA} C^2_{\chi^0\chi^0 A}}{(s - m_A^2)^2 + m_A^2\Gamma_A^2} \frac{s^2}{16\pi} \sqrt{1 + \frac{4m_f^2}{s}}, \qquad \text{(A1)}$$

$$\omega^H_{f\bar{f}} = \frac{C^2_{ffH} C^2_{\chi^0\chi^0 H}}{(s-m_H^2)^2 + m_H^2\Gamma_H^2} \frac{(s-4m^2_{\chi^0})(s-4m_f^2)}{16\pi} \sqrt{1+\frac{4m_f^2}{s}}. \tag{A2}$$

Here the label H denotes either CP-even Higgs boson. C_{ffA}, $C_{\chi^0\chi^0 A}$, C_{ffH} and $C_{\chi^0\chi^0 H}$ are the fermion-fermion-Higgs and neutralino-neutralino-Higgs couplings. $\Gamma_{A,H}$ are the widths of the respective Higgs bosons.

These squared amplitudes can be used to attain the thermally averaged annihilation cross section [40]

$$\langle\sigma v\rangle = \frac{\omega(s_0)}{m^2_{\chi^0}} - \frac{3}{m_{\chi^0}}\left[\frac{\omega(s_0)}{m^2_{\chi^0}} - 2\omega'(s_0)\right]T + \mathcal{O}(T^2) = \frac{1}{m^2_{\chi^0}}\left[1-\frac{3T}{m_{\chi^0}}\right]\omega(s)\Big|_{s\to 4m^2_{\chi^0}+6m_{\chi^0}T} + \mathcal{O}(T^2), \tag{A3}$$

where T is the temperature. Keeping terms to zeroth and first order in T is sufficient for the relic abundance calculation. Writing this as an expansion in $x = T/m_{\chi^0}$, $\langle\sigma v\rangle = a + bx + \mathcal{O}(x^2)$, we arrive at

$$\begin{aligned}
a_{\chi\chi\to A\to f\bar{f}} &= \frac{g_2^4 c_f m_f^2 \tan^2\beta}{8\pi m_W^2} \frac{m^2_{\chi^0}\sqrt{1-m_f^2/m^2_{\chi^0}}}{(4m^2_{\chi^0}-m_A^2)^2 + m_A^2\Gamma_A^2}[\epsilon_U(\epsilon_W - \epsilon_B\tan\theta_W)\sin\beta - \epsilon_D(\epsilon_W - \epsilon_B\tan\theta_W)\cos\beta]^2,\\
b_{\chi\chi\to A\to f\bar{f}} &= 0, \qquad a_{\chi\chi\to H\to f\bar{f}} = 0,\\
b_{\chi\chi\to H\to f\bar{f}} &= \frac{3g_2^4 c_f m_f^2 \cos^2\alpha}{16\pi m_W^2\cos^2\beta} \frac{(m^2_{\chi^0}-m_f^2)\sqrt{1-m_f^2/m^2_{\chi^0}}}{(4m^2_{\chi^0}-m_H^2+im_H\Gamma_H)^2}[\epsilon_U(\epsilon_W - \epsilon_B\tan\theta_W)\cos\alpha - \epsilon_D(\epsilon_W - \epsilon_B\tan\theta_W)\sin\alpha]^2,\\
a_{\chi\chi\to h\to f\bar{f}} &= 0,\\
b_{\chi\chi\to h\to f\bar{f}} &= \frac{3g_2^4 c_f m_f^2 \sin^2\alpha}{16\pi m_W^2\cos^2\beta} \frac{(m^2_{\chi^0}-m_f^2)\sqrt{1-m_f^2/m^2_{\chi^0}}}{(4m^2_{\chi^0}-m_h^2+im_h\Gamma_h)^2}[\epsilon_U(\epsilon_W - \epsilon_B\tan\theta_W)\sin\alpha - \epsilon_D(\epsilon_W - \epsilon_B\tan\theta_W)\cos\alpha]^2,
\end{aligned} \tag{A4}$$

where c_f is a color factor, equal to 3 for quarks and 1 for leptons. The quantities $\epsilon_{B,W,U,D}$ are the components of the lightest neutralino which are b-ino, W-ino, up-type Higgsino and down-type Higgsino, respectively. These expressions assume that the final state fermions are down type. For up-type fermions the factor of $\tan^2\beta$ should be replaced by $\cot^2\beta$.

[1] R. Barate *et al.* (ALEPH Collaboration), Phys. Lett. B **565**, 61 (2003); A. Heister *et al.* (ALEPH Collaboration), Phys. Lett. B **526**, 191 (2002).

[2] M. Drees, Phys. Rev. D **71**, 115006 (2005).

[3] For early attempts in this direction see also M. Carena, J. R. Ellis, A. Pilaftsis, and C. E. M. Wagner, Phys. Lett. B **495**, 155 (2000); A. Sopczak, Int. J. Mod. Phys. A **16S1B**, 816 (2001); Yad. Fiz. **65**, 2179 (2002) [Phys. At. Nucl. **65**, 2116 (2002)]; Nucl. Phys. B, Proc. Suppl. **109**, 271 (2002); G. Weiglein, hep-ph/0108063.

[4] See e.g. J. F. Gunion and A. Turski, Phys. Rev. D **39**, 2701 (1989); **40**, 2333 (1989); M. S. Berger, Phys. Rev. D **41**, 225 (1990); R. Hempfling and A. H. Hoang, Phys. Lett. B **331**, 99 (1994); we are using the formulas as in A. Krause, T. Plehn, M. Spira, and P. M. Zerwas, Nucl. Phys. **B519**, 85 (1998).

[5] M. Carena, J. R. Espinosa, M. Quiros, and C. E. M. Wagner, Phys. Lett. B **355**, 209 (1995).

[6] S. Heinemeyer, W. Hollik, and G. Weiglein, Comput. Phys. Commun. **124**, 76 (2000); G. Degrassi, S. Heinemeyer, W. Hollik, P. Slavich, and G. Weiglein, Eur. Phys. J. C **28**, 133 (2003).

[7] K. Abe *et al.* (Belle Collaboration), Phys. Lett. B **511**, 151 (2001); B. Aubert *et al.* (*BABAR* Collaboration), hep-ex/0207076; S. Chen *et al.* (CLEO Collaboration), Phys. Rev. Lett. **87**, 251807 (2001); R. Barate *et al.* (ALEPH Collaboration), Phys. Lett. B **429**, 169 (1998); H. F. A. Group (HFAG), hep-ex/0505100.

[8] P. L. Cho, M. Misiak, and D. Wyler, Phys. Rev. D **54**, 3329 (1996); J. L. Hewett and J. D. Wells, Phys. Rev. D **55**, 5549 (1997); F. M. Borzumati and C. Greub, Phys. Rev. D **58**, 074004 (1998); **59**, 057501 (1999); G. Hiller and F. Kruger, Phys. Rev. D **69**, 074020 (2004).

[9] L. J. Hall, R. Rattazzi, and U. Sarid, Phys. Rev. D **50**, 7048 (1994); M. Carena, M. Olechowski, S. Pokorski, and C. E. Wagner, Nucl. Phys. **B426**, 269 (1994); M. Carena, D. Garcia, U. Nierste, and C. E. Wagner, Nucl. Phys. **B577**, 88 (2000); J. Guasch, P. Hafliger, and M. Spira, Phys. Rev. D **68**, 115001 (2003).

[10] For a recent reference see A. J. Buras, Phys. Lett. B **566**, 115 (2003).

[11] J. L. Hewett, S. Nandi, and T. G. Rizzo, Phys. Rev. D **39**, 250 (1989); M. J. Savage, Phys. Lett. B **266**, 135 (1991); C. Bobeth, T. Ewerth, F. Kruger, and J. Urban, Phys. Rev.

D **64**, 074014 (2001); A. Dedes, H. K. Dreiner, U. Nierste, and P. Richardson, hep-ph/0207026.

[12] D. Acosta *et al.* (CDF Collaboration), Phys. Rev. Lett. **93**, 032001 (2004); V. M. Abazov *et al.* (D0 Collaboration), Phys. Rev. Lett. **94**, 071802 (2005).

[13] See e.g. M. Calvi, in Proceedings of the Rencontres de Moriond, 2005 (to be published).

[14] G. W. Bennett *et al.* (Muon g-2 Collaboration), Phys. Rev. Lett. **92**, 161802 (2004); R. R. Akhmetshin *et al.* (CMD-2 Collaboration), Phys. Lett. B **578**, 285 (2004).

[15] M. Davier, S. Eidelman, A. Hocker, and Z. Zhang, Eur. Phys. J. C **31**, 503 (2003); F. Jegerlehner, Nucl. Phys. B, Proc. Suppl. **126**, 325 (2004); K. Hagiwara, A. D. Martin, D. Nomura, and T. Teubner, Phys. Rev. D **69**, 093003 (2004).

[16] A. Aloisio *et al.* (KLOE Collaboration), Phys. Lett. B **606**, 12 (2005); G. Rodrigo, H. Czyz, J. H. Kuhn, and M. Szopa, Eur. Phys. J. C **24**, 71 (2002).

[17] M. Krawczyk, hep-ph/0103223.

[18] A. Czarnecki and W. J. Marciano, Phys. Rev. D **64**, 013014 (2001); S. P. Martin and J. D. Wells, Phys. Rev. D **64**, 035003 (2001); **67**, 015002 (2003); for a more recent calculation see also S. Heinemeyer, D. Stockinger, and G. Weiglein, Nucl. Phys. **B699**, 103 (2004).

[19] G. Belanger, F. Boudjema, A. Pukhov, and A. Semenov, hep-ph/0405253.

[20] J. R. Ellis, J. S. Hagelin, D. V. Nanopoulos, K. A. Olive, and M. Srednicki, Nucl. Phys. **B238**, 453 (1984); H. Goldberg, Phys. Rev. Lett. **50**, 1419 (1983); for a review of neutralino dark matter, see G. Jungman, M. Kamionkowski, and K. Griest, Phys. Rep. **267**, 195 (1996); G. Bertone, D. Hooper, and J. Silk, Phys. Rep. **405**, 279 (2005).

[21] C. L. Bennett *et al.*, Astrophys. J. Suppl. Ser. **148**, 1 (2003).

[22] D. S. Akerib *et al.* (CDMS Collaboration), Phys. Rev. Lett. **93**, 211301 (2004).

[23] GERDA proposal, http://wwwgerda.mppmu.mpg.de/

[24] H. Wang, in Proceedings of Dark Matter 2004, Marina del Ray (to be published).

[25] O. Martineau, in Proceedings of Dark Matter 2004, Marina del Ray (to be published).

[26] P. Gondolo, J. Edsjo, P. Ullio, L. Bergstrom, M. Schelke, and E. A. Baltz, J. Cosmol. Astropart. Phys. 07 (2004) 008.

[27] L. Bergstrom, J. Edsjo, and P. Ullio, Phys. Rev. Lett. **87**, 251301 (2001); D. Hooper and B. L. Dingus, Phys. Rev. D **70**, 113007 (2004); L. Bergstrom, P. Ullio, and J. H. Buckley, Astropart. Phys. **9**, 137 (1998); L. Wai *et al.* (GLAST LAT Collaboration), New Astron. Rev. **49**, 307 (2005); A. Morselli, Nucl. Phys. B, Proc. Suppl. **134**, 127 (2004); AIP Conf. Proc. **745**, 422 (2005); Eur. Phys. J. C **33**, S978 (2004).

[28] E. A. Baltz and J. Edsjo, Phys. Rev. D **59**, 023511 (1999); S. Profumo and P. Ullio, J. Cosmol. Astropart. Phys. 07 (2004) 006; D. Hooper and J. Silk, Phys. Rev. D **71**, 083503 (2005); M. Circella (PAMELA Collaboration), Nucl. Instrum. Methods Phys. Res., Sect. A **518**, 153 (2004); P. Spillantini, Nucl. Instrum. Methods Phys. Res., Sect. B **214**, 116 (2004); K. Scholberg, Nucl. Phys. B, Proc. Suppl. **138**, 35 (2005); M. Sapinski, Eur. Phys. J. C **33**, S975 (2004).

[29] T. Plehn, D. L. Rainwater, and D. Zeppenfeld, Phys. Lett. B **454**, 297 (1999); Phys. Rev. D **61**, 093005 (2000).

[30] S. Abdullin *et al.*, Eur. Phys. J. C **39S2**, 41 (2005); S. Asai *et al.*, Eur. Phys. J. C **32S2**, 19 (2004); V. Buscher and K. Jakobs, Int. J. Mod. Phys. A **20**, 2523 (2005); for a recent update see also K. Cranmer, in Proceedings of the North American ATLAS Physics Workshop (to be published).

[31] T. Plehn, D. L. Rainwater, and D. Zeppenfeld, Phys. Rev. Lett. **88**, 051801 (2002).

[32] E. Boos, A. Djouadi, M. Muhlleitner, and A. Vologdin, Phys. Rev. D **66**, 055004 (2002); E. Boos, A. Djouadi, and A. Nikitenko, Phys. Lett. B **578**, 384 (2004).

[33] K. A. Assamagan and Y. Coadou, Acta Phys. Pol. B **33**, 707 (2002); K. A. Assamagan, Y. Coadou, and A. Deandrea, Eur. Phys. J. direct C **4**, 1 (2002); D. Denegri *et al.*, hep-ph/0112045; S. Raychaudhuri and D. P. Roy, Phys. Rev. D **53**, 4902 (1996); R. M. Barnett, H. E. Haber, and D. E. Soper, Nucl. Phys. **B306**, 697 (1988); S. H. Zhu, Phys. Rev. D **67**, 075006 (2003); T. Plehn, Phys. Rev. D **67**, 014018 (2003).

[34] F. Borzumati, J. L. Kneur, and N. Polonsky, Phys. Rev. D **60**, 115011 (1999); E. L. Berger, T. Han, J. Jiang, and T. Plehn, Phys. Rev. D **71**, 115012 (2005).

[35] K. A. Assamagan, M. Guchait, and S. Moretti, hep-ph/0402057.

[36] J. A. Coarasa, J. Guasch, J. Sola, and W. Hollik, Phys. Lett. B **442**, 326 (1998).

[37] C. Biscarat, Report No. ATL-SLIDE-2003-002; S. Banerjee and M. Maity, J. Phys. G **28**, 2443 (2002).

[38] V. M. Abazov *et al.* (D0 Collaboration), Phys. Rev. Lett. **88**, 151803 (2002).

[39] Exact analytic cross sections for neutralino-neutralino annihilations and coannihilations into two and three body states are given in A. Birkedal-Hansen and E. h. Jeong, J. High Energy Phys. 02 (2003) 047.

[40] J. R. Ellis, T. Falk, K. A. Olive, and M. Srednicki, Astropart. Phys. **13**, 181 (2000); **15**, 413(E) (2001).